Molecular Assemblies

DOI: 10.1002/anie.200905503

Supramolecular Assemblies Formed on an Epitaxial Graphene Superstructure**

Andrew J. Pollard, Edward W. Perkins, Nicholas A. Smith, Alex Saywell, Gudrun Goretzki, Anna G. Phillips, Stephen P. Argent, Hermann Sachdev, Frank Müller, Stefan Hüfner, Stefan Gsell, Martin Fischer, Matthias Schreck, Jürg Osterwalder, Thomas Greber, Simon Berner, Neil R. Champness, and Peter H. Beton**

The seminal work of Novoselov et al.[1] has stimulated great interest in the controllable growth of epitaxial graphene monolayers.[2–12] While initial research was focussed on the use of SiC wafers,[3] the promise of transition metals as substrates has also been demonstrated[4–12] and both approaches are scalable to large-area production.[4,5,8,12] The growth of graphene on transition metals such as Ru, Rh and Ir leads to a moiré-like superstructure,[6,7,9,10,12,13] similar to that observed for BN monolayers.[14,15] Here we show that such a superstructure can be used to control the organization of extended supramolecular nanostructures. The formation of two-dimensional supramolecular arrays has received increasing attention over recent years primarily due to potential applications in nanostructure fabrication as well as fundamental interest in self-assembly processes.[16–18] Such studies can be highly dependent on the nature of the substrate used, and the interplay between surface and adsorbed supramolecular structure is a topic of significant conjecture. Until now metallic surfaces[17] or highly oriented pyrolytic graphite (HOPG)[18] have typically been the surfaces of choice for such studies. Our results demonstrate that graphene is compatible with, and can strongly influence molecular self-assembly.

We have studied the adsorption of perylene tetracarboxylic diimide (PTCDI) and related derivatives on a graphene monolayer grown on a Rh(111) heteroepitaxial thin film (Figure 1). In particular, we show that a near-commensurability between the PTCDI molecular dimensions and a moiré-like superstructure leads to the stabilization of extended one-dimensional supramolecular assemblies. The stabilization is due to NH···O intermolecular hydrogen bonds between imide groups on neighboring molecules.[19,20] This interaction may be systematically modified by the attachment

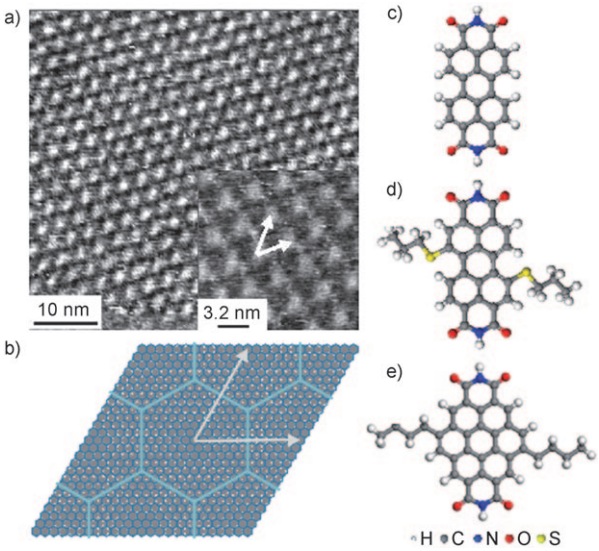

Figure 1. a) STM image of graphene monolayer on Rh(111)/YSZ/Si(111) substrate (sample voltage 1.0 V, tunnel current 200 pA). The periodic features (period 2.95 nm) arise from a moiré pattern because of the mismatch between the graphite and Rh lattice constants. b) Diagram of honeycomb mesh (dark blue) representing graphene overlaid on an array of gray circles representing Rh atoms. The superstructure formed by 12×12 unit cells of graphene overlaid on 11×11 unit cells of Rh gives rise to a long range periodic pattern (unit cell highlighted in light blue) with lattice vectors marked by arrows—these are also identified in the zoomed image shown in the inset to (a). c–e) Structure of the three molecules under investigation: c) PTCDI, d) DP-PTCDI, e) DB-CTCDI.

[*] A. J. Pollard, Dr. E. W. Perkins, N. A. Smith, A. Saywell, Prof. P. H. Beton
School of Physics & Astronomy, University of Nottingham
Nottingham, NG7 2RD (UK)
E-mail: peter.beton@nottingham.ac.uk
Dr. G. Goretzki, A. G. Phillips, Dr. S. P. Argent, Prof. N. R. Champness
School of Chemistry, University of Nottingham
Nottingham, NG7 2RD (UK)
E-mail: Neil.Champness@nottingham.ac.uk
Priv.-Doz. H. Sachdev, Dr. F. Müller
Anorganische und Allgemeine Chemie
Universität des Saarlandes, Saarbrücken (Germany)
Dr. F. Müller, Prof. S. Hüfner
Institut für Experimentalphysik
Universität des Saarlandes, Saarbrücken (Germany)
Dr. S. Gsell, M. Fischer, Dr. M. Schreck
Institut für Physik, Universität Augsburg (Germany)
Prof. J. Osterwalder, Prof. T. Greber, Dr. S. Berner
Physik-Institut, Universität Zürich (Switzerland)

[**] We are grateful to the financial support under grant EP/D048761/1 from the UK Engineering and Physical Sciences Research Council. The initial collaboration resulted from financial support from EU grant NMP4-CT-2004-013817 "Nanomesh". We are grateful to Luis Perdigao for discussions related to density functional calculations.
Supporting information for this article is available on the WWW under http://dx.doi.org/10.1002/anie.200905503.

of alkane chains to the "bay" area of the fused aromatic core resulting in a stabilization of a triangular, rather than linear, molecular junction. Specifically we investigate 1,7-dipropylthio-perylene-3,4:9,10-tetracarboxydiimide (DP-PTCDI) (Figure 1 d)[21] and 1,7-di(butyl)-coronene-3,4:9,10-tetracarboxylic acid bisimide (DB-CTCDI; Figure 1 e; see Ref. [22] and Supporting Information for synthetic details).

Our experiments were performed under ultra-high vacuum (UHV) conditions using scanning tunnelling microscopy (STM; operated at room temperature) as the primary experimental technique. The preparative procedures for the Rh(111) substrate are described in detail elsewhere[12] (see also Ref. [23]). In summary, a heteroepitaxial yttria-stabilized zirconia (YSZ) buffer layer is first grown on a Si(111) wafer. A Rh thin film (150 nm) is then grown on the YSZ buffer layer. A piece of the wafer (area ca. 1 cm^2) is cleaned in UHV using a cycle of Ar ion sputtering followed by annealing in a partial pressure of oxygen (see Supporting Information). To form a graphene monolayer we first extract the sample from UHV, then immerse it in an organic solvent (acetone or paraldehyde ($C_6H_{12}O_3$)) for 10–15 seconds and then return it to the UHV system. After gradually annealing up to ca. 500 °C over 24 h the sample is heated to 800 °C for 30 min resulting in the formation of a graphene monolayer. This method of graphene production has provided insights into the mechanism of formation of epitaxial graphene. Investigations using low energy electron diffraction, photoelectron spectroscopy and STM support a model in which the precursor molecules undergo a decomposition process with dicarbon species (C_2 radicals) as intermediates, which then finally combine to form a graphene monolayer.[12] An STM image acquired following this procedure shows clearly the superstructure arising from the moiré pattern associated with the graphene monolayer (see STM image and diagram in Figure 1 a and b). The superstructure arises from 12×12 graphene unit cells overlaid on 11×11 Rh(111) unit cells and has an overall period, $a_m = 2.95$ nm.[12]

Figure 2 a shows an STM image acquired (see Supporting Information for experimental details) after deposition of PTCDI in which rows with a width corresponding to one molecule and lengths up to 25 nm are clearly resolved running parallel to the principal directions of the surface. There are many examples of pairs of extended rows which are adsorbed on neighboring sites of the moiré superstructure with a spacing of $\sqrt{3}a_m/2$, although this appears to be the minimum spacing for neighboring rows. The molecular arrangement on the graphene superstructure differs significantly from that observed for a graphite substrate, on which three-dimensional islands are formed and the PTCDI/substrate interface is buried, precluding a direct comparison with the ordering observed here.[24] Single-molecule rows of PTCDI have been observed on Ag passivated silicon, but these rows are short and unstable and are rapidly converted to two-dimensional islands.[19] The PTCDI morphology also differs significantly from that reported for C_{60} and other organic molecules on a SiC/graphene "nanomesh", where close-packed two-dimensional islands are observed.[25]

Previous experimental estimates of the spacing of molecules within PTCDI rows range from 1.41–1.46 nm.[19] Noting

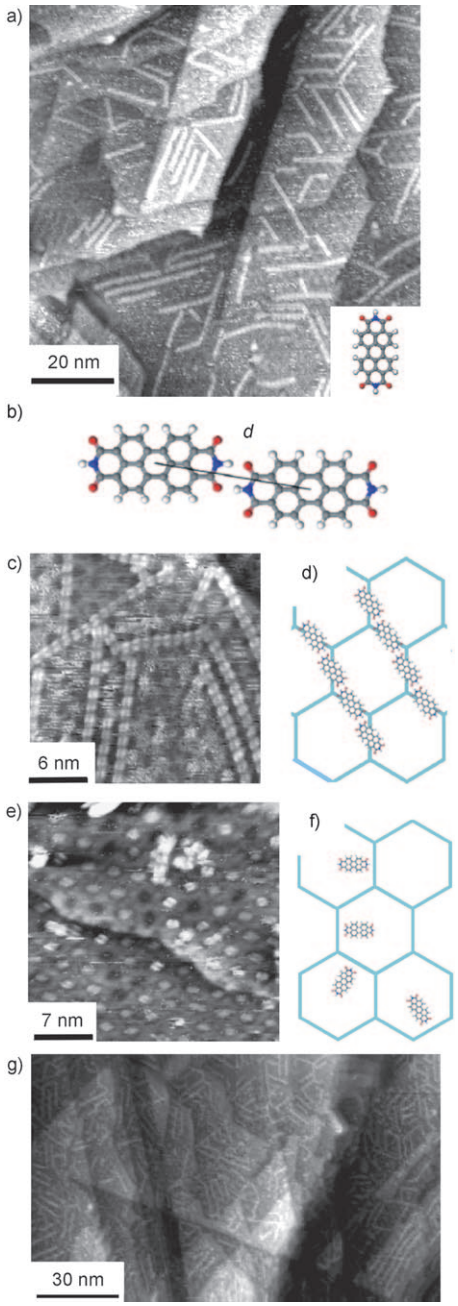

Figure 2. a) STM image acquired following deposition of PTCDI on a graphene monolayer formed on Rh(111)/YSZ/Si(111); inset: structure of deposited molecule. b) PTCDI–PTCDI dimer with a center–center separation of *d* stabilized by two hydrogen bonds. c) Small area scan showing intramolecular double lobe contrast of PTCDI molecules on graphene. d) Placement of PTCDI rows on graphene superstructure as depicted in Figure 1 b. e) STM image of PTCDI on a BN nanomesh formed on Rh(111)/YSZ/Si(111) in which isolated molecules are trapped in nanomesh "pores" in contrast to the rows formed on graphene. f) Placement of molecules on BN nanomesh. g) Higher coverage of PTCDI (0.11 molecules nm^{-2}) showing prevalence of molecular rows spaced regularly on graphene. Imaging parameters are: a) −1 V, tunnel current 200 pA; d) −1 V, 150 pA; e) −1.7 V, 30 pA; f) −1 V, 200 pA.

the near match between this spacing and $a_m/2$ (1.47 ± 0.05 nm) of the graphene superstructure, we propose below a structural model for commensurate PTCDI rows (Figure 2b–d). Figure 2c shows an STM image of PTCDI in which intramolecular features are resolved in the form of two bright lobes which run parallel to the long axis of symmetry of the molecule. These lobes have previously been shown to correspond to the highest occupied molecular orbital (HOMO)[19] of PTCDI and allow us to confirm that the orientation of the molecule and its placement on the graphene superstructure is in agreement with the proposed model in Figure 2d.

The importance of a commensurate match between molecular dimensions and the moiré periodicity is highlighted by a comparison (see Figure 2e) with adsorption of PTCDI on a boron nitride "nanomesh" monolayer[14] also formed on the Rh(111)/YSZ/Si(111) surface (see Supporting Information). This monolayer is isoelectronic with graphene, and also displays a moiré pattern but with a slightly larger periodicity of 3.2 nm which does not have a simple commensurability with the molecular dimensions. On this surface we observe individual isolated PTCDI molecules (Figure 2f) trapped in energy minima associated with the moiré pattern very similar to that reported previously for napthalocyanine on the same surface.[15] We attribute the absence of extended PTCDI structures on this surface to the lack of commensurability between the rows and the BN superstructure. Consequently, molecules cannot be adsorbed in positions where they minimize, independently, their energies of interaction with both the surface and their neighboring molecules. The double lobe intramolecular structure is also resolved for molecules adsorbed on the BN nanomesh, from which we deduce that there is no preferred in-plane orientation. In contrast, on graphene, we do not observe isolated PTCDI and the molecular orientation is non-random. The commensurability on the graphene surface leads to the formation of continuous rows, and the stabilization of the molecule in an orientation directed at a neighboring occupied site.

The deposition of DP-PTCDI (Figure 3a) also leads to the formation of commensurate rows, but, as compared with PTCDI, there are fewer examples of pairs of parallel rows and there are many more junctions where three molecules meet (the ratio of dimer:trimer junctions is 75:25; for PTCDI less than 1% of junctions are trimers). For DB-CTCDI the formation of analogous junctions between three molecules dominates (we are not able to identify unambiguously any

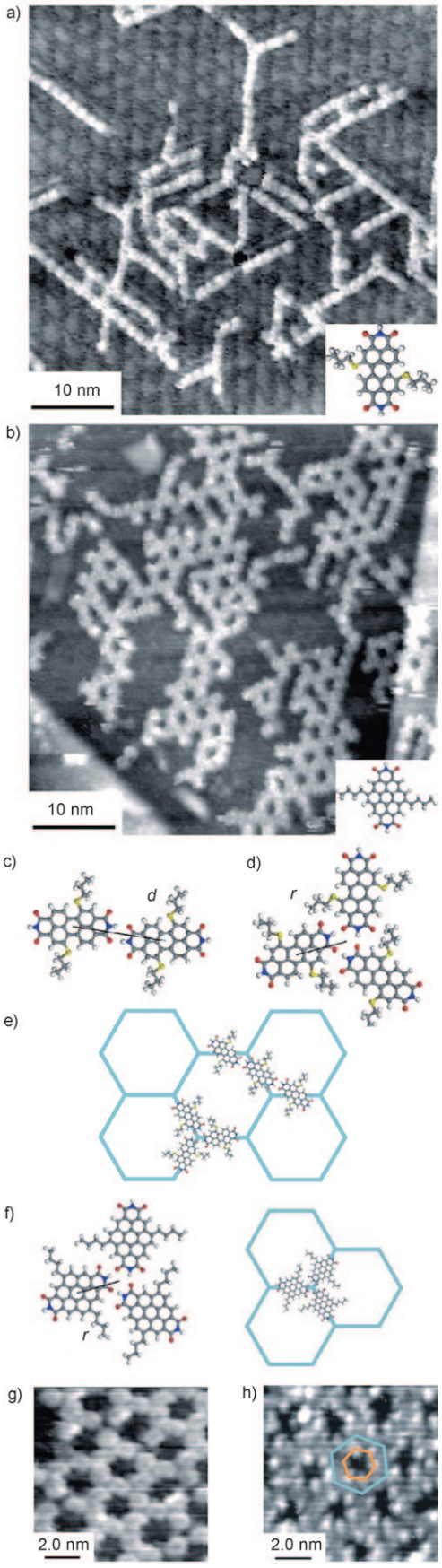

Figure 3. STM images acquired following deposition of a) DP-PTCDI, b) DB-CTCDI on a graphene monolayer formed on Rh(111)/YSZ/Si(111). c, d) Diagram of junctions between DP-PTCDI dimers (c) and trimers (d) stabilized, respectively, by two and three C=O···NH hydrogen bonds between neighboring molecules with dimer center–center spacing of *d* and trimer vertex to molecule center spacing *r*. e) Placement of DP-PTCDI trimers and dimers. f) DB-CTCDI trimer junction analogous to (d) with vertex to molecule center spacing *r* and placement of DB-CTCDI trimer on the graphene superstructure. g, h) STM images of DB-CTCDI showing chirality of junctions and intramolecular detail of molecules. The hexagons in (h) highlight the chirality of the molecular arrangement. Imaging parameters: a) −1.0 V, 100 pA; b) 1.0 V, 100 pA; g) 1.5 V, 50 pA; h) −1.5 V, 50 pA.

linear dimers) the observed molecular arrangements (Figure 3b). The array of trimers results in a honeycomb arrangement of molecules which is aligned with the graphene monolayer superstructure and encloses the areas of bright contrast arising from the moiré pattern.

The presence of alkyl side-chains is known from previous studies of DP-PTCDI to enhance the stability of a chiral molecular trimer vertex (illustrated in Figure 3d) as compared with the linear hydrogen-bonded PTCDI-PTCDI junctions.[22] A comparison of Figures 2a and 3a,b indicates a progressively enhanced stabilization of a trimer vertex as the alkyl chain length increases from zero length (PTCDI) through to the longest chain (DB-CTCDI). This leads to a change in morphology from the rows, for PTCDI, through to the honeycomb DB-CTCDI, with the DP-PTCDI being considered as an intermediate case where linear segments co-exist with junctions of three molecules. The enhanced stability of the trimer vertex for molecules with longer alkane chains is supported by density functional theory (DFT) calculations (performed in the gas-phase in the absence of the substrate; see Supporting Information) as summarized in Table 1 which shows the greatest difference between trimer and dimer binding energies is predicted for DB-CTCDI. These data also indicate that, in the gas phase, the trimer is more stable for DP-PTCDI and even for PTCDI. An additional contribution to the stabilization energy arises due to the van der Waals interactions of the alkyl chains, but is not captured in the DFT calculations. This is estimated, using classical force fields (see Supporting Information) applied to the optimized geometries calculated using DFT. We find that, for DP-PTCDI and DB-CTCDI, the difference in energies between trimers and dimers is increased by ca. 0.2 eV due to the presence of the alkyl chains.

Table 1: Calculated binding energies, intermolecular separations d and vertex separations $2r$.[a]

	E^{d}_{HB} [eV]	d [nm]	E^{t}_{HB} [eV]	$2r$ [nm]	$E^{t}_{HB}-E^{d}_{HB}$ [eV] (DFT)
PTCDI	0.46	1.44	0.52	1.61	0.06
DP-PTCDI	0.46	1.45	0.57	1.63	0.11
DB-CTCDI	0.45	1.44	0.57	1.60	0.12

[a] E^{d}_{HB}: energy per molecule in a row of dimers; E^{t}_{HB}: energy per molecule in an extended honeycomb array of trimers. The values are calculated as described in the Supporting Information. The relative stability of the trimers over the dimers shows a trend of increasing stability from PTCDI to DB-CTCDI, which is consistent with our experimental observations. Also tabulated are the calculated intermolecular separations for the dimer, d, and the vertex separation, $2r$, for the trimer (see Figures 2 and 3 for definition of distances).

Also tabulated in Table 1 are the calculated separations of the intermolecular junctions. For dimers formed from all of the molecules investigated, the calculated equilibrium separation is very close (within 0.03 nm) to $a_m/2$ (the observed spacing of molecules in the commensurate rows is 1.47 ± 0.05 nm). However, the predicted separation for intermolecular trimer junctions (Table 1) is significantly lower (by up to 0.1 nm) than their expected separation in an extended array, $a_m/\sqrt{3}$ (1.70 ± 0.06 nm). Thus, we expect these junctions to be strained in an extended honeycomb array, leading to a reduced binding energy, and propose that this accounts for the stability of rows for the two molecules PTCDI and DP-PTCDI, whereas only the molecule with the strongest predicted trimer junction, DB-CTCDI forms a honeycomb array.

The images in Figures 2 and 3 show clearly that the adsorbed molecules experience a local potential due to the graphene superstructure which is sufficiently strong to inhibit the formation of two-dimensional islands. The origin of this potential has recently been discussed by Brugger et al.[13] who showed that for both graphene and boron nitride monolayers on Ru(0001) (closely related to Rh(111)) variations in local work function lead to a periodic potential. However, the topography of the resulting potentials which arise for graphene and BN show significant differences. In particular, for graphene on Ru(0001) the high symmetry points (equivalent to the centers of the light blue hexagon in Figure 1b) were shown to be energy maxima, while the energy minima were shown to form a honeycomb network corresponding to a connected region following, approximately, the edges of the light blue hexagon in Figure 1b). In contrast, molecular adsorption on BN occurs preferentially approximately midway between the center and edge of the unit cell of the moiré superstructure as previously discussed by Dil et al.[26] The placement of molecules which we observe is in excellent agreement with the different potential landscapes arising from the homoatomic character of graphene and the heteroatomic character of BN, respectively, as discussed by Brugger et al.[13]

There are parallels with other systems where molecules or clusters are adsorbed at sites on an ordered array of local potential wells arising from self-organization due to, for example, surface reconstruction or dislocation arrays,[27–29] including those adsorbed on boron nitride[15] and graphene monolayers.[6] However a distinguishing feature of our work is the observation that the trapping potential is sufficiently compliant to allow the molecules to relax and adopt a local configuration which is controlled by interactions with molecules trapped in neighboring energy minima so that extended, connected structures may be formed. This represents an example of a system which exhibits hierarchies of order,[30] since the formation of the molecular rows is determined by intermolecular interactions but the placement and separation of the rows is guided by the underlying level of organization due to the moiré pattern. The control of row separation is shown in Figure 2a and more clearly for a higher molecular coverage in Figure 2g.

The attachment of alkane chains to DP-PTCDI and DB-CTCDI leads to a surface-induced chirality[31] for these molecules. Furthermore, the trimer junction is intrinsically chiral. Images of the DB-CTCDI network shown in Figures 3g and h confirm that the molecules are in a chiral arrangement (both chiralities have been observed with domain sizes of up to 30 nm). Specifically in Figure 3h the bright intramolecular features form a hexagon with an axis of symmetry rotated with respect to the principal axes of the

molecular network (which are parallel to those of the graphene superstructure). Note also that there are clear gaps between some of the trimers in Figures 3 g and h—further evidence of strain arising from a small mismatch between molecular and superstructure dimensions for the trimer array.

Our results show that graphene superstructures offer a suitable substrate for the formation of extended, hierarchical self-assembled nanostructures. In addition to the intrinsic interest in self-assembly processes our work also raises interesting questions in relation to graphene electronics. Recent papers have demonstrated that molecules can act as molecular dopants[32] and also that the superstructure resulting from a moiré pattern of graphene grown on Ir(111) gives rise to the formation of a band-gap[33] raising interesting connections with the self-assembled molecular structures we report here. The interplay between the characteristic dimensions resulting from graphene growth and molecular ordering offer many possible routes for further investigation related to both the electronic properties of graphene as well as the formation of complex self-assembled structures.

Received: October 1, 2009
Revised: November 23, 2009
Published online: February 4, 2010

Keywords: graphene · hydrogen-bonding · molecular recognition · supramolecular assembly

[1] a) K. S. Novoselov, A. K. Geim, S. V. Morozov, D. Jiang, Y. Zhang, S. V. Dubonos, I. V. Grigorieva, A. A. Firsov, *Science* **2004**, *306*, 666 – 669; b) A. K. Geim, *Science* **2009**, *324*, 1530 – 1534.

[2] C. N. R. Rao, A. K. Sood, K. S. Subrahmanyam, A. Govindaraj, *Angew. Chem.* **2009**, *121*, 7890 – 7916; *Angew. Chem. Int. Ed.* **2009**, *48*, 7752 – 7777.

[3] C. Berger, Z. Song, T. Li, X. Li, A. Y. Ogbazghi, R. Feng, Z. Dai, A. N. Marchenkov, E. H. Conrad, P. N. First, W. A. de Heer, *J. Phys. Chem. B* **2004**, *108*, 19912 – 19916.

[4] K. S. Kim, Y. Zhao, H. Jang, S. Y. Lee, J. M. Kim, K. S. Kim, J.-H. Ahn, P. Kim, J.-Y. Choi, B. H. Hong, *Nature* **2009**, *457*, 706 – 710.

[5] A. Reina, X. Jia, J. Ho, D. Nezich, H. Son, V. Bulovic, M. S. Dresselhaus, J. Kong, *Nano Lett.* **2009**, *9*, 30 – 35.

[6] J. Coraux, A. T. N'Diaye, C. Busse, T. Michely, *Nano Lett.* **2008**, *8*, 565 – 570.

[7] P. W. Sutter, J.-I. Flege, E. A. Sutter, *Nat. Mater.* **2008**, *7*, 406 – 411.

[8] Q. Yu, J. Lian, S. Siriponglert, H. Li, Y. P. Chen, S.-S. Pei, *Appl. Phys. Lett.* **2008**, *93*, 113103; A. J. Pollard, R. R. Nair, S. N. Sabki, C. R. Staddon, L. M. A. Perdigao, C. H. Hsu, J. M. Garfitt, S. Gangopadhyay, H. F. Gleeson, A. K. Geim, P. H. Beton, *J. Phys. Chem. C* **2009**, *113*, 16565 – 16567.

[9] A. T. N'Diaye, J. Coraux, T. N. Plasa, C. Busse, T. Michely, *New J. Phys.* **2008**, *10*, 043033.

[10] D. Martoccia, P. R. Willmott, T. Brugger, M. Björck, S. Günther, C. M. Schlepütz, A. Cervellino, S. A. Pauli, B. D. Patterson, S. Marchini, J. Wintterlin, W. Moritz, T. Greber, *Phys. Rev. Lett.* **2008**, *101*, 126102.

[11] D. Usachov, A. M. Dobrotvorskii, A. Varykhalov, O. Rader, W. Gudat, A. M. Shikin, V. K. Adamchuk, *Phys. Rev. B* **2008**, *78*, 085403.

[12] F. Müller, H. Sachdev, S. Hüfner, A. J. Pollard, E. W. Perkins, J. C. Russell, P. H. Beton, S. Gsell, M. Fischer, M. Schreck, B. Strizker, *Small* **2009**, *5*, 2291 – 2296.

[13] T. Brugger, S. Günther, B. Wang, J. H. Dil, M.-L. Bocquet, J. Osterwalder, J. Wintterlin, T. Greber, *Phys. Rev. B* **2009**, *79*, 045407.

[14] M. Corso, W. Auwarter, M. Muntwiler, A. Tamai, T. Greber, J. Osterwalder, *Science* **2004**, *303*, 217 – 220.

[15] S. Berner, M. Corso, R. Widmer, O. Groening, R. Laskowski, P. Blaha, K. Schwarz, A. Goriachko, H. Over, S. Gsell, M. Schreck, H. Sachdev, T. Greber, J. Osterwalder, *Angew. Chem.* **2007**, *119*, 5207 – 5211; *Angew. Chem. Int. Ed.* **2007**, *46*, 5115 – 5119.

[16] a) J. V. Barth, G. Costantini, K. Kern, *Nature* **2005**, *437*, 671 – 679; b) T. Kudernac, S. Lei, J. A. A. W. Elemans, S. De Feyter, *Chem. Soc. Rev.* **2009**, *38*, 402 – 421; c) J. Sakamoto, J. van Heijst, O. Lukin, A. D. Schlüter, *Angew. Chem.* **2009**, *121*, 1048 – 1089; *Angew. Chem. Int. Ed.* **2009**, *48*, 1030 – 1069.

[17] a) J. A. Theobald, N. S. Oxtoby, M. A. Phillips, N. R. Champness, P. H. Beton, *Nature* **2003**, *424*, 1029 – 1031; b) A. Llanes-Pallas, M. Matena, T. Jung, M. Prato, M. Stöhr, D. Bonifazi, *Angew. Chem.* **2008**, *120*, 7840 – 7844; *Angew. Chem. Int. Ed.* **2008**, *47*, 7726 – 7730; c) M. E. Cañas-Ventura, W. Xiao, D. Wasserfallen, K. Müllen, H. Brune, J. V. Barth, R. Fasel, *Angew. Chem.* **2007**, *119*, 1846 – 1850; *Angew. Chem. Int. Ed.* **2007**, *46*, 1814 – 1818; d) L. M. A. Perdigão, N. R. Champness, P. H. Beton, *Chem. Commun.* **2006**, 538 – 540; e) P. A. Staniec, L. M. A. Perdigão, A. Saywell, N. R. Champness, P. H. Beton, *ChemPhysChem* **2007**, *8*, 2177 – 2181.

[18] a) M. O. Blunt, J. Russell, M. C. Giménez-López, J. P. Garrahan, X. Lin, M. Schröder, N. R. Champness, P. H. Beton, *Science* **2008**, *322*, 1077 – 1081; b) M. Blunt, X. Lin, M. C. Gimenez-Lopez, M. Schröder, N. R. Champness, P. H. Beton, *Chem. Commun.* **2008**, 2304 – 2306; c) V. Stepanenko, F. Würthner, *Small* **2008**, *4*, 2158 – 2161; d) M. Li, S.-B. Lei, Y.-L. Yang, T.-S. Wang, Y.-T. Shen, C.-R. Wang, Q.-D. Zeng, C. Wang, *Angew. Chem.* **2008**, *120*, 6819 – 6823; *Angew. Chem. Int. Ed.* **2008**, *47*, 6717 – 6721; e) C. Meier, K. Landfester, D. Künzel, T. Markert, A. Groß, U. Ziener, *Angew. Chem.* **2008**, *120*, 3881 – 3885; *Angew. Chem. Int. Ed.* **2008**, *47*, 3821 – 3825; f) S. Lei, K. Tahara, F. C. De Schryver, M. Van der Auweraer, Y. Tobe, S. De Feyter, *Angew. Chem.* **2008**, *120*, 3006 – 3010; *Angew. Chem. Int. Ed.* **2008**, *47*, 2964 – 2968.

[19] J. C. Swarbrick, J. Ma, J. A. Theobald, N. S. Oxtoby, J. N. O'Shea, N. R. Champness, P. H. Beton, *J. Phys. Chem. B* **2005**, *109*, 12167 – 12174; D. L. Keeling, N. S. Oxtoby, C. Wilson, M. J. Humphry, N. R. Champness, P. H. Beton, *Nano Lett.* **2003**, *3*, 9 – 12.

[20] C. Ludwig, B. Gompf, J. Petersen, R. Strohmaier, W. Eisenmenger, *Z. Phys. B* **1994**, *93*, 365 – 373.

[21] L. M. A. Perdigão, A. Saywell, G. N. Fontes, P. A. Staniec, G. Goretzki, N. R. Champness, P. H. Beton, *Chem. Eur. J.* **2008**, *14*, 7600 – 7607.

[22] F. Nolde, W. Pisula, S. Müller, C. Kohl, K. Müllen, *Chem. Mater.* **2006**, *18*, 3715 – 3725.

[23] S. Gsell, M. Fischer, M. Schreck, B. Stritzker, *J. Cryst. Growth* **2009**, *311*, 3731 – 3736.

[24] N. Berdunov, A. J. Pollard, P. H. Beton, *Appl. Phys. Lett.* **2009**, *94*, 043110.

[25] W. Chen, H. L. Zhang, H. Xu, E. S. Tok, K. P. Loh, A. T. S. Wee, *J. Phys. Chem. B* **2006**, *110*, 21873 – 21881; Q. H. Wang, M. C. Hersam, *Nat. Chem.* **2009**, *1*, 206 – 211.

[26] H. Dil, J. Lobo-Checa, R. Laskowski, P. Blaha, S. Berner, J. Osterwalder, T. Greber, *Science* **2008**, *319*, 1824 – 1826.

[27] W. Xiao, P. Ruffieux, K. Aït-Mansour, O. Gröning, K. Palotas, W. A. Hofer, P. Gröning, R. Fasel, *J. Phys. Chem. B* **2006**, *110*, 21394 – 21398.

[28] N. Weiss, T. Cren, M. Epple, S. Rusponi, G. Baudot, S. Rohart, A. Tejeda, V. Repain, S. Rousset, P. Ohresser, F. Scheurer, P. Bencok, H. Brune, *Phys. Rev. Lett.* **2005**, *95*, 157204; H. Brune, M. Giovannini, K. Broman, K. Kern, *Nature* **1998**, *394*, 451 – 453.
[29] B. Lu, T. Iimori, K. Sakamoto, K. Nakatsuji, F. Rosei, F. Komori, *J. Phys. Chem. C* **2008**, *112*, 10187 – 10192.
[30] V. Palermo, P. Samori, *Angew. Chem.* **2007**, *119*, 4510 – 4514; *Angew. Chem. Int. Ed.* **2007**, *46*, 4428 – 4432.
[31] Q. Chen, D. J. Frankel, N. V. Richardson, *Surf. Sci.* **2002**, *497*, 37 – 46.
[32] W. Chen, S. Chen, D. C. Qi, X. Y. Gao, A. T. S. Wee, *J. Am. Chem. Soc.* **2007**, *129*, 10418 – 10422.
[33] I. Pletikosić, M. Kralj, P. Pervan, R. Brako, J. Coraux, A. T. N'Diaye, C. Busse, T. Michely, *Phys. Rev. Lett.* **2009**, *102*, 056808.

